

Thermophysical properties of paramagnetic Fe from first principles

Hossein Ehteshami^{1,*} and Pavel A. Korzhavii^{1,2}

¹*Department of Materials Science and Engineering, KTH Royal Institute of Technology, SE-10044 Stockholm, Sweden*

²*Materials Modeling and Development Laboratory, National University of Science and Technology "MISIS", 119049 Moscow, Russia*

(Received 11 January 2017; revised manuscript received 9 October 2017; published 5 December 2017)

A computationally efficient, yet general, free-energy modeling scheme is developed based on first-principles calculations. Finite-temperature disorder associated with the fast (electronic and magnetic) degrees of freedom is directly included in the electronic structure calculations, whereas the vibrational free energy is evaluated by a proposed model that uses elastic constants to calculate *average* sound velocity of the quasiharmonic Debye model. The proposed scheme is tested by calculating the lattice parameter, heat capacity, and single-crystal elastic constants of α -, γ -, and δ -iron as functions of temperature in the range 1000–1800 K. The calculations accurately reproduce the well-established experimental data on thermal expansion and heat capacity of γ - and δ -iron. Electronic and magnetic excitations are shown to account for about 20% of the heat capacity for the two phases. Nonphonon contributions to thermal expansion are 12% and 10% for α - and δ -Fe and about 30% for γ -Fe. The elastic properties predicted by the model are in good agreement with those obtained in previous theoretical treatments of paramagnetic phases of iron, as well as with the bulk moduli derived from isothermal compressibility measurements [N. Tsujino *et al.*, *Earth Planet. Sci. Lett.* **375**, 244 (2013)]. Less agreement is found between theoretically calculated and experimentally derived single-crystal elastic constants of γ - and δ -iron.

DOI: [10.1103/PhysRevB.96.224406](https://doi.org/10.1103/PhysRevB.96.224406)

I. INTRODUCTION

Iron and its alloys are widely used as engineering materials in many branches of industry. One reason is that their physical and chemical properties can be tuned to the requirements of a specific application by additional alloying, as well as by means of thermal, chemical, and mechanical treatment. This, in turn, is possible because of the multitude of structural states (and transitions between them) in iron alloys that can be controlled by changing the composition, temperature, and pressure. Experimentally, it is known that the low-temperature body-centered-cubic (bcc) phase of iron, α -Fe, undergoes a phase transition to the face-centered-cubic (fcc) γ -Fe phase at 1185 K and, subsequently, γ -Fe transforms to another bcc phase, δ -Fe, at 1667 K [1]. In addition to these structural transitions, the magnetic transition in iron is known to have an impact on metallurgy of iron and its alloys [2,3].

Thermophysical properties of high-temperature phases are of practical importance in connection with high-temperature applications of stainless steel and also because the manufacturing routes of various grades of steel include thermal and/or mechanical treatments in the austenitic region. In particular, elastic properties measure the mechanical stiffness of a material and determine the velocities of sound waves in it. Changes in the microstructure or phase composition generally lead to changes in the wave propagation characteristics (sound velocity and damping coefficient), which can be exploited for nondestructive testing and characterization of materials using ultrasonic methods [4]. To use such methods for characterization of metals/alloys, one should have *a priori* knowledge about the variation of elastic properties with temperature and composition.

Despite their importance, experimental data on the elastic properties of γ - and δ -Fe are very scarce. There is just one study reporting the whole set of single-crystal elastic constants of γ -Fe, C_{11} , C_{12} , and C_{44} , at 1428 K, evaluated from phonon dispersion relations obtained in the neutron-scattering experiments by Zarestky and Stassis [5]. The situation is similar for δ -Fe, for which there is only one set of data available [6]. A temperature dependence of the isothermal bulk modulus of γ -Fe has been obtained by extrapolating the data of compressibility measurements by Tsujino *et al.* using a high-temperature Birch-Murnaghan equation of state [7].

Where experimental data are lacking due to difficulties of high-temperature measurements, first-principles calculations may provide the necessary information. Recent progress in the elastic property calculations using first-principles methods is reviewed in Refs. [8,9]. The case of paramagnetic Fe is complicated because this case requires special treatment of its finite-temperature paramagnetism [10–13]. Spin-unpolarized density functional theory calculations, treating paramagnetic iron as nonmagnetic, are practically useless because they strongly underestimate the equilibrium volume and overestimate elastic constants of γ -Fe (see Table I). As the Table I also shows, a dynamical mean-field theory (DMFT) treatment of finite-temperature paramagnetism yields elastic constants [10] that are quite similar, in terms of agreement with the experimental elastic constants of α -Fe and γ -Fe, to the results obtained within the disordered local moment (DLM) model of the paramagnetic state [15,16].

In this paper, we show how the equilibrium volume, elastic constants, and other relevant thermophysical properties of α -, γ -, and δ -Fe can be derived from first principles using a systematic approach based on a model of the free energy that includes electronic, magnetic, and vibrational contributions, taking into account their quantum nature. Our free-energy model is, in essence, a quasiharmonic Debye model that has been extended to systems exhibiting paramagnetic disorder of atomic spin

*heht@kth.se

TABLE I. Experimental and calculated elastic constants (GPa) of PM bcc and fcc Fe. The theoretical values correspond to non-spin-polarized calculations treating γ -Fe as nonmagnetic (NM) and to finite-temperature treatments of paramagnetism using the dynamical mean-field theory (DMFT) or the disordered local moment (DLM) model.

	T	C_{44}	C'	C_{11}
α -Fe				
Experiment ^a	1173	99	13	149
Experiment ^b	1173	118	12	190
Theory, ^c NM		119	-187	-15
Theory, ^c DMFT	1252	127	36	230
Theory, ^d DLM	1200	129	19	157
Theory, ^e DLM	1200	109	16	
This work, DLM	1200	110	20	151
γ -Fe				
Experiment ^f	1428	77 ± 8	16 ± 14	154 ± 14
Experiment ^b	1573	68	18	171
Theory, ^c NM		197	73	223
Theory, ^c DMFT	1460	138	25	210
Theory, ^d DLM	1400	138	28	127
Theory, ^e DLM	1400	112	23	
This work, DLM	1428	124	24	136
δ -Fe				
Experiment ^b	1743	86	11	158
This work, DLM	1750	98	18	128

^aUltrasonic measurements, Ref. [14].

^bNeutron scattering, Ref. [6].

^cGGA-based calculations, Ref. [10].

^dGGA-based calculations, Ref. [15].

^eGGA-based calculations, Ref. [16].

^fInelastic neutron scattering, Ref. [5].

moments, and it enables us to study thermophysical properties of high-temperature phases of iron.

II. METHODOLOGY

A. Electronic and magnetic free-energy models

In the present model, the free-energy contributions due to electronic, magnetic, and vibrational disorder at finite temperatures are taken into account in the following order. First, the electronic free energy, including the energy and entropy effects due to excitations of valence electrons from below to above the Fermi level, is calculated by introducing the Fermi-Dirac distribution function,

$$f_T(\epsilon) = [e^{(\mu-\epsilon)/kT} + 1]^{-1}, \quad (1)$$

into all the complex energy integrals used in the electronic structure calculations [17,18] and taking residues at the Matsubara poles of $f_T(\epsilon)$,

$$\epsilon_j = \mu \pm i\pi(2j-1)kT, \quad j = 1, 2, \dots, N_{\text{res}}, \quad (2)$$

that are enclosed by the integration contour. Here ϵ is complex energy, μ is the Fermi level, k is the Boltzmann constant, and T is the electronic temperature. The contour extends from below the valence band to a cutoff energy some $2\pi N_{\text{res}}kT$ above the Fermi level. Typically, the number of Matsubara poles N_{res}

is chosen to be between 4 and 8. An additional integration over the same energy contour is carried out to evaluate the electronic entropy,

$$S_{\text{el}} = -k \int \{f_T \ln f_T + [1 - f_T] \ln [1 - f_T]\} n(\epsilon) d\epsilon, \quad (3)$$

where $n(\epsilon)$ is the electron density of states expressed in terms of the single-particle Green's function. For brevity, the dependence of f_T on energy is omitted in Eq. (3).

The magnetic free-energy contribution is evaluated within the DLM model of the paramagnetic state, which is in line with simplified theoretical interpretations of experimental data [19,20] and is further corroborated by recent spin-spiral calculations showing weak dependencies of the Fe magnetic moment and total energy on the spiral wave vector [21,22]. The electronic structure and energy of a random DLM state are calculated using the coherent potential approximation (CPA) [23,24] to represent a pseudobinary alloy consisting of Fe atoms with spin-up (\uparrow) and spin-down (\downarrow) local moments distributed randomly on the underlying lattice (alloy analogy) [25,26]. The entropy due to the magnetic moment disorder is taken into account in the paramagnetic lattice gas (PLG) form:

$$S_{\text{mag}} = k \ln(m+1). \quad (4)$$

Here m is the average magnitude of the local spin moment on an Fe atom [27]. For metals, m is a continuously varying quantity, but let us note that for an integer (i.e., truly localized) spin moment the value $m+1$ gives the multiplicity (the number of possible projections of the moment on the spin axis). Importantly, for thermodynamic modeling, the PLG form of magnetic entropy, Eq. (4), is a smoothly varying, convex function of m , and it correctly vanishes in the nonmagnetic state with $m=0$, whose multiplicity is 1.

A self-consistent treatment of paramagnetic disorder requires that the partial free energy, including the $-TS_{\text{mag}}$ term, should be minimized. Considering an atomic spin moment m as the imbalance of spin-up and spin-down electron densities (site projected and integrated over the atomic volume) and introducing a local spin coordinate framework, we note that the magnitude m can be varied by additionally splitting up the on-site one-electron potential with a constant shift $\Delta U_{\uparrow,\downarrow} = \pm \Delta U$. Linearizing around the initial value m_0 , one gets $(m - m_0) \approx C \Delta U$ for the change in the moment and $(E - E_0) \approx (\Delta U)^2 / 2C$ for the corresponding change in one-electron energy. Here C is an effective susceptibility, and E_0 is the unperturbed energy. Minimizing the partial free energy $E - TS_{\text{mag}}$, one gets a closed expression for the potential shift:

$$\Delta U_{\uparrow,\downarrow} = \pm kT / (|m| + 1). \quad (5)$$

This temperature-dependent contribution to the one-electron potential is a mean-field description of the tendency of the magnitude of a localized magnetic moment to increase with temperature as a result of *transverse* spin fluctuations in the DLM paramagnetic state [27,28]. This tendency stems from the fact that a larger paramagnetic moment has a greater multiplicity, thereby producing a higher entropy, Eq. (4). Figure 1 shows the variation of the Fe magnetic moment as induced by temperature, calculated as discussed above. The

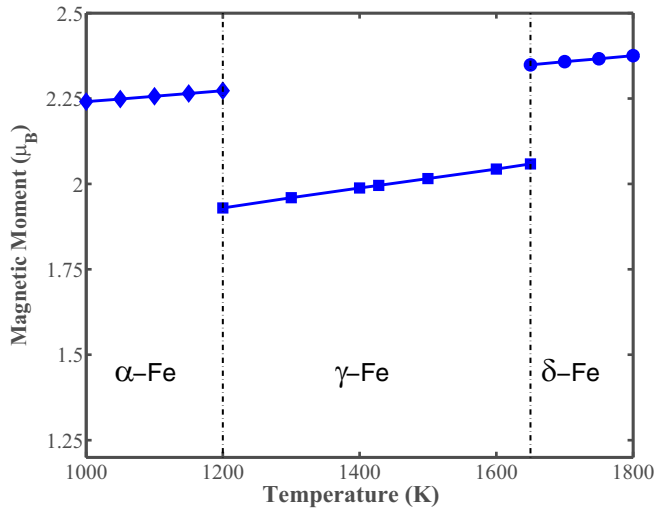


FIG. 1. Magnetic moment μ_B of α -, γ -, and δ -Fe as a function of temperature.

increase of m is partly due to the thermal expansion (see Sec. III A).

A note should be added about the usage of the DLM-PLG model. Strictly speaking, it is applicable to atoms and ions with well-developed paramagnetic moments in a disordered state well above the magnetic ordering temperature. For example, the model should be capable of describing the anti-Invar type of behavior that is characteristic of γ -Fe. The model can also describe the situation when an atom in a metallic host forms a paramagnetic moment by localizing a valence-band electron (Mott transition). However, the model should be applied with caution to atoms whose moments vanish in the DLM calculations as $T \rightarrow 0$: if the temperature-induced moments are not sizable and there is no alternative (e.g., experimental) evidence of local-moment paramagnetic behavior in the system, then the treatment of such moments as localized is unjustified.

Also, the DLM-PLG model partly accounts for *longitudinal* spin fluctuations (LSFs), but only as long as the parabolic form $(E - E_0) \approx C(m - m_0)^2/2$ can be considered a good approximation. For systems exhibiting nonlinear $E(m)$ dependencies (in particular, for Invar alloys) and, in general, for all systems at very high temperatures, more accurate treatments of LSF are necessary. LSFs have been the subject of several studies [16,21,29–35], but it remains to be seen how their results can be combined with the present model without breaking the good analytic properties of the thermodynamic functions and at a reasonable computational cost.

However, the magnetic free-energy contribution is relatively small, and its approximate treatment may be sufficient for describing the thermophysical properties of paramagnetic Fe. As will be shown in Sec. III, the vibrational and electronic free-energy contributions account for more than 85% of the heat capacity and linear thermal expansion coefficient. Therefore, considering the purpose of the present study, correct approximations for the vibrational contribution seem to be paramount for a successful thermodynamic modeling of iron phases at elevated temperatures.

B. Debye model and computational procedure

The effect of lattice vibrations, which is the primary cause of thermal expansion, is evaluated in this work using the quasiharmonic Debye model with a single parameter (Debye temperature) that is both volume- and temperature-dependent. The dependencies have been calculated from the finite-temperature equation of state that already includes the electronic and magnetic free-energy contributions. This treatment is consistent with the general coarse-graining approach where the dynamics corresponding to slow degrees of freedom (atomic motions, in this case) are described using the potential-energy surface obtained as a partial free energy by equilibrating the system with respect to the fast degrees of freedom (electronic and magnetic). However, this treatment is not *self-consistent*, as it does not take into account the effect of atomic displacements on the electronic structure. Feedback from the atomic displacements into the electronic structure may play a crucial role in cases of dynamically unstable phases such as β -Ti, and it can be taken into account using several different schemes at a considerable computational cost [13,26,36]. As paramagnetic phases of Fe are dynamically stable in the DLM-PLG treatment, their vibrational free energies are expected to be accurately described by the quasiharmonic Debye model.

Technical details of the present calculations, based on density functional theory [37], were as follows. The total energies were calculated within the generalized gradient approximation [38] (GGA) using the exact muffin-tin orbital (EMTO) method [39–41] and the full-charge-density formalism [41,42]. Self-consistent EMTO-CPA calculations were performed using an orbital momentum cutoff of $l_{\max} = 3$ for partial waves and a $33 \times 33 \times 33$ Monkhorst-Pack grid of special k points [43] for the Brillouin zone integration.

The electronic structure calculations for a set of temperatures in the range from 1000 to 1800 K for bcc and fcc Fe yielded the the partial “electronic” Helmholtz free energy $F_{ei}(V, T)$ containing the electronic and magnetic contributions. From the so-obtained equation of state, for every considered value of temperature T and volume V , the vibrational energy $E_D(V, T)$ and entropy $S_D(V, T)$ were evaluated as follows:

$$E_D(V, T) = \frac{9}{8}\Theta_D + 3kTD(\Theta_D/T), \quad (6)$$

$$S_D(V, T) = k[4D(\Theta_D/T) - 3\ln(1 - e^{-\Theta_D/T})], \quad (7)$$

where $D(x) = (3/x^3) \int_0^x dt [t^3/(e^t - 1)]$ is the Debye function. The Debye temperature $\Theta_D(V, T)$ was determined in the framework of the Debye model through the *mean* sound velocity $v_m(V, T)$, namely,

$$\Theta_D = \frac{\hbar}{k} \left(\frac{6\pi^2}{V} \right)^{1/3} v_m(V, T). \quad (8)$$

The mean sound velocity was calculated by averaging the three acoustic branches over directions in the crystal lattice, viz.,

$$v_m(V, T) = \left(\frac{1}{3} \sum_{i=1}^3 \int_{\Omega} \frac{1}{v_i^3} \frac{d\Omega}{4\pi} \right)^{-\frac{1}{3}}, \quad (9)$$

where $d\Omega$ is an increment of the solid angle about the center of the Brillouin zone and v_i are longitudinal and transverse

sound velocities. It is desirable to find some approximations for the equation above in order to simplify the calculations. For example, for isotropic crystals [44] this relation simplifies to

$$v_m = \left(\frac{1}{3} \left[\frac{2}{v_s^3} + \frac{1}{v_l^3} \right] \right)^{-\frac{1}{3}}, \quad (10)$$

where v_s and v_l are transverse (shear) and longitudinal sound velocities, respectively. Considering an empirical linear relationship between longitudinal and shear sound velocities with the square root of the bulk modulus, Moruzzi, Janak, and Schwarz [45] suggested a formula to evaluate the Debye temperature; their formalism is hereafter referred to as MJS. While the MJS formalism has been quite successful in predicting the thermophysical properties of several metals, our calculations show that the MJS formalism works quite well for γ -Fe but strongly overestimates the main thermophysical properties of δ -Fe.

Another common practice is to use homogenization theories employing Voigt, Reuss, or Hill (VRH) averages to relate the single-crystal elastic constants to mean sound velocities; for an example see Ref. [33]. Our test calculations for α -, γ -, and δ -iron show that experimental thermophysical properties of γ -Fe can be reproduced using the VRH average, while the lattice expansion and other thermal properties of δ -Fe are underestimated.

One possible reason for the high sensitivity of thermal properties of δ -Fe to the Debye model formulation of MJS is the very high value of the Zener anisotropy constant ($A = C_{44}/C'$) for δ -Fe [6]. In cases of strong elastic anisotropy, the usage of Eq. (10) is rather questionable because in such cases some directions of sound propagation will be much softer than others, so the assumption that all directions of sound propagation are similar cannot be justified. One can also add to the above the fact that, at high temperatures, vibrational modes with short wavelengths (and high frequencies) are more populated than at low temperatures and therefore play an increasingly important role.

Following this rationale, our approach is to find an effective sound velocity that would represent the contributions of high-frequency modes, as well as low-frequency modes, to the vibrational free energy. Examining Eq. (9), one can see that the softest vibrational mode, the lowest shear mode, is dominant in the determination of this integral. Dominance of the softest mode is more pronounced at high temperatures since in such a situation one has softening of all elastic moduli due to temperature. To work around this issue, we have introduced a modified theory to calculate the effective sound velocity as follows. For each direction in an irreducible wedge of the Brillouin zone (BZ), we have calculated the three acoustic sound velocities. Once the velocities of the three acoustic branches are known, the projection of the velocity of each branch on one of the principal axes can be calculated. Since the cubic phases are the focus of our study, three principal axes in this study are three mutually perpendicular axes. This procedure is repeated for all directions confined to the irreducible part of the BZ. As soon as the projections of velocities are known, for each principal axis an average is obtained. As a result, v_m can be simply obtained from the

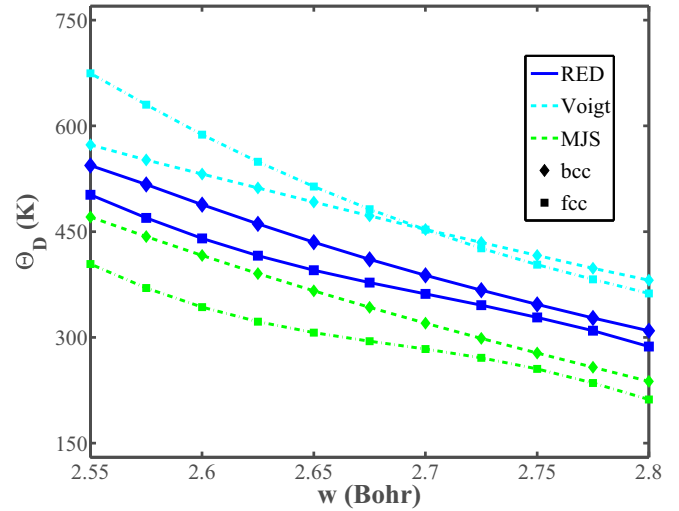


FIG. 2. Debye temperature Θ_D (K) as a function of Wigner-Seitz radius w (bohrs) calculated using different methods. For the bcc phase, Θ_D is calculated at a constant temperature of 1700 K, and for the fcc phase it is calculated at 1400 K.

three averages on the principal axes. Having calculated the averages on each axis, one can view the result as a direction and interpret it as a resultant effective direction (RED).

By calculating the single-crystal elastic constants from partial free energies, as will be discussed in Sec. III C, for a range of volumes and temperatures, one can obtain v_m from the above procedure as a function of volume and temperature. Figure 2 shows the variation of the Debye temperature Θ_D calculated using the RED approximation, MJS formalism, and Voigt average as a function of the Wigner-Seitz radius w at a fixed temperature. One can see that the values obtained from the RED lie somewhere in between those obtained using the Voigt average and MJS formalism. For the fcc structure, differences between different approximations are rather large at a lower Wigner-Seitz radius, while for the bcc structure, different methods give similar results. Surprisingly, the large difference between the three different estimates of Θ_D for the fcc structure, especially at lower volumes, do not affect the properties at high temperature as much as might be expected from Fig. 2. The opposite is true for the bcc structure, where more similar estimates of Θ_D translate into more differing results for the properties. This is an example of the nontriviality of high-temperature modeling of thermophysical properties. Figure 3 shows the variation of Θ_D as a function of temperature calculated for α -, γ -, and δ -Fe at a fixed Wigner-Seitz radius. The trend observed in Fig. 2 is seen here again for the different methods to estimate Θ_D . The main observation of Fig. 3 is that Θ_D is almost independent of temperature for all three phases: the value of Θ_D changes by 0.8 K in whole temperature range for the bcc phases and by the same amount for the fcc phase within the temperature range of its stability.

Having calculated Θ_D as a function of volume and temperature, the vibrational energy $E_D(V, T)$ and entropy $S_D(V, T)$ contributions can be evaluated according to Eqs. (6)

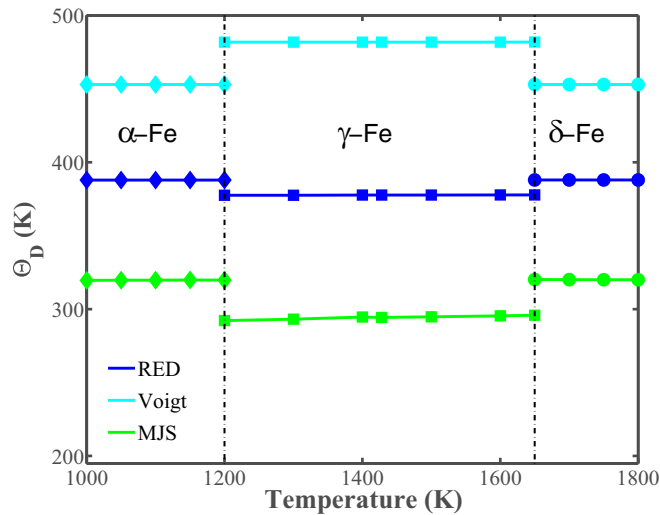


FIG. 3. Debye temperature Θ_D (K) computed using different methods for α -, γ -, and δ -Fe as a function of temperature. For the bcc phase, Θ_D is calculated at a fixed Wigner-Seitz radius of 2.725 bohrs, and for the fcc phase it is calculated at 2.675 bohrs.

and (7). The total free energy

$$F(V, T) = F_{el}(V, T) + E_D(V, T) - T S_D(V, T),$$

including these contributions, is then calculated and fitted as a function of volume and temperature. Basic thermophysical properties such as the equilibrium volume $V_0(T)$ and lattice parameter $a(T)$, thermal expansion coefficient (TEC), isothermal bulk modulus B_T , and isobaric heat capacity $C_P(T)$ can be calculated using the corresponding derivatives of the free energy.

III. RESULTS AND DISCUSSION

A. Thermal expansion

The calculated Wigner-Seitz radii w , representing the equilibrium volumes $V_0 = 4\pi w^3/3$ of the three phases of Fe, are plotted as functions of temperature in Fig. 4. The calculations systematically underestimate the experimental data (also shown in Fig. 4), on average by about 0.3%, 1.3%, and 0.2% for α -, γ -, and δ -Fe, respectively. Although the agreement between the modified theory and experiment appears now to be good for α - and δ -Fe, the discrepancy for γ -Fe is still appreciable. This discrepancy is expected and may be traced back to a common problem of semilocal density functionals to underestimate the equilibrium volume of iron [47]. At the same time, the calculated slopes of temperature dependencies are similar to the experimental observations.

In Table II the calculated linear TECs are compared with the experimental values [46]. In the modified theory the TEC is slightly overestimated for α -Fe and underestimated for γ -Fe. The agreement is seemingly good for δ -Fe. It also follows from the results shown in Table II that the contribution of electronic and magnetic excitations to TEC for α - and δ -Fe is about 12% and 10% of the total values, respectively, while these nonphonon excitations contribute about 30% to the lattice expansion for γ -Fe. It can therefore be concluded that while phonons are the primary cause of lattice expansion,

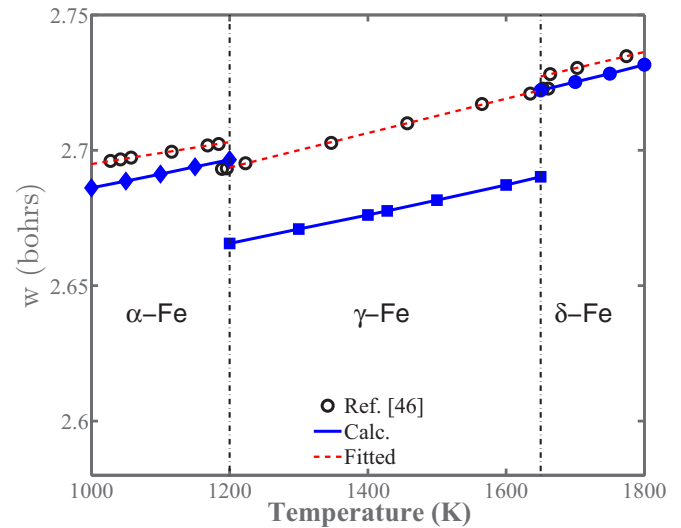


FIG. 4. Wigner-Seitz radius w (bohrs) of α -, γ -, and δ -Fe as a function of temperature. Experimental data (open circles) are taken from lattice parameter measurements of Ref. [46] and their linear regression (dashed lines) for α -Fe, $w(T) = 2.65433 + 4.05835 \times 10^{-5} T$; γ -Fe, $w(T) = 2.61754 + 6.34387 \times 10^{-5} T$; and δ -Fe, $w(T) = 2.62790 + 6.02238 \times 10^{-5} T$. Solid lines with solid symbols show the calculated temperature dependencies of the Wigner-Seitz radius for α -, γ -, and δ -Fe, from left to right.

their role in the thermal expansion of α - and δ -Fe is more substantial than in that of γ -Fe. We would like to add to the above discussion that a possible overestimation of the linear TEC for α -Fe could be due to the fact that at intermediate and low temperatures, statistically, the higher-frequency modes are not as highly populated as at high temperature and the RED approximation may not be as suitable as the other two higher-temperature phases.

B. Heat capacity

The calculated isobaric ($P = 0$) heat capacity and its contributions due to the vibrational and electronic degrees

TABLE II. Calculated and experimental linear TEC of paramagnetic bcc and fcc phases of Fe. All data are in units of 10^{-6} K^{-1} and have been averaged over the temperature range of stability of the corresponding paramagnetic phase.

	This work	Theory ^a	Experiment ^b
α -Fe			
Total	19.5	16.5	14.8
El.+mag. ^c	2.3		
γ -Fe			
Total	19.1	27.2	23.3
El.+mag. ^c	5.5		
δ -Fe			
Total	23.8		22.1
El.+mag. ^c	2.3		

^aDLM-based Debye model, Ref. [33].

^bLattice parameter measurements, Ref. [46].

^cExpansion due to electronic and magnetic excitations.

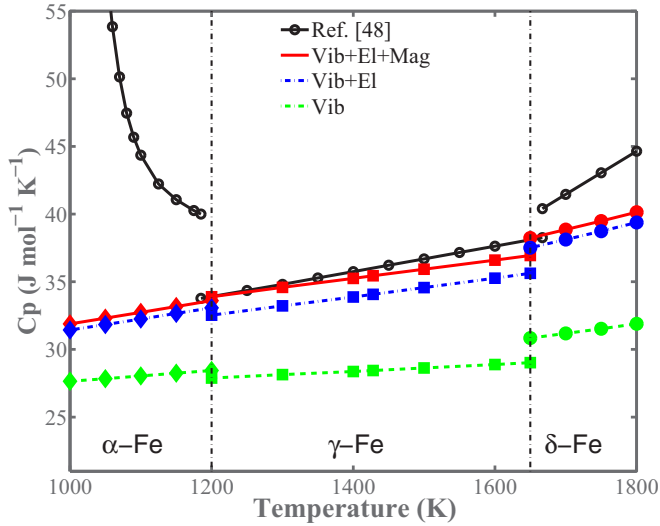


FIG. 5. Calculated heat capacity C_p and its contributions as functions of temperature. Experimental points are taken from Ref. [48] to represent the results of a critical assessment of a large number of experimental data.

of freedom are shown in Fig. 5. Due to the difficulties with experiments at elevated temperatures, raw experimental data for γ -Fe and δ -Fe show large scatter. Desai [48] critically assessed a large number of experimental data and suggested a set of recommended values which are plotted in Fig. 5. The agreement between the calculated and assessed experimental data is very good for γ -Fe and is rather good for δ -Fe. The calculations slightly underestimate the slope of the heat capacity at the high-temperature end for both phases of γ and δ . The underestimation for δ -Fe is greater, and it can be related to other contributions that become significant at high temperatures. There is a substantial difference between the calculated and experimental heat capacities of paramagnetic α -Fe. The reason for the substantial underestimation of the heat capacity for α -Fe is the absence of magnetic short-range order contributions in our CPA treatment of DLM paramagnetism, while these contributions are quite sizable just above the magnetic phase transition temperature $T_c \sim 1043$ K in α -Fe. The greatest contribution to the heat capacity comes from lattice vibrations (harmonic and anharmonic terms together). The smallest contribution comes from magnetic disorder and is related to the increasing magnitude of spin fluctuations with temperature [27]. In the considered temperature range the contribution of nonphonon degrees of freedom (electronic and magnetic) to the total heat capacity is about 19%.

C. Elastic properties

To calculate the three cubic elastic constants as functions of temperature, one needs two independent elastic moduli in addition to the temperature-dependent bulk modulus $B = (C_{11} + 2C_{12})/3$. A common choice is to calculate two shear moduli $C' = (C_{11} - C_{12})/2$ and C_{44} by homogeneously shearing the lattice at a fixed (equilibrium) volume [49]. The so-called tetragonal shear constant C' is calculated by imposing a volume-conserving orthorhombic strain for which the strain tensor ϵ is expressed in terms of a small displacement

parameter x as follows:

$$\epsilon_{11} = -\epsilon_{22} = x, \quad \epsilon_{33} = \frac{x^2}{1-x^2}. \quad (11)$$

The resulting energy difference is an even function of the parameter x :

$$\Delta F(x) = \Delta F(-x) = 2V_0 C' x^2 + O[x^4]. \quad (12)$$

Similarly, using a volume-conserving monoclinic strain, the C_{44} modulus can be calculated. The strain tensor in this case is

$$\epsilon_{12} = \epsilon_{21} = \frac{x}{2}, \quad \epsilon_{33} = \frac{x^2}{4-x^2}, \quad (13)$$

and, once again, the corresponding energy difference is an even function of x :

$$\Delta F(x) = \Delta F(-x) = V_0 C_{44} x^2 / 2 + O[x^4]. \quad (14)$$

A series of calculations was performed to consider the volume-conserving lattice distortions (11) and (13) at the *calculated equilibrium volume* $V_0(T)$ corresponding to a given temperature T . The maximum strain x_{\max} of 0.06 (dimensionless) was divided into several steps to calculate the partial free energy $F_{el}(x)$ at the given T and $V_0(T)$. The shear elastic constants $C_{44}(T)$ and $C'(T)$ were then calculated from the slope of the partial free energy as a function of the strain squared x^2 according to Eqs. (12) and (14).

The elastic constants calculated in this work for paramagnetic bcc and fcc Fe for several temperatures are compared in Table I with the corresponding experimental data of Refs. [5,6,14] and the results of previous theoretical investigations [10,15,16]. The values obtained in this work are similar to the results of other calculations treating paramagnetic Fe. For α -Fe, our results seem to be slightly closer to the experimental data, especially for C_{11} reported in Ref. [14]. For γ -Fe, the calculated C' is in good agreement with the experimental data of Refs. [5,6], but C_{11} is underestimated in comparison with the data from Ref. [6].

It seems to be a general trend for theoretical calculations to overestimate C_{44} of the γ phase. It should also be added that while C_{44} and C' of Ref. [6] are in the same range as the experimental data of Refs. [5,14] for α - and γ -Fe, C_{11} reported in Ref. [6] is higher than in the two other experiments.

Our results for the δ phase are also in good agreement with the only available experimental data for this phase [6]. At variance with the previous studies, the present model incorporates the effect of lattice vibrations (in the quasiharmonic Debye model) on the elastic properties.

Figure 6 compares the calculated temperature dependencies of two shear moduli, C_{44} and C' , and isothermal bulk modulus B_T with available experimental data for α -, γ -, and δ -Fe. Similar to the experimental B_T obtained in Refs. [7,14], the calculated elastic moduli exhibit a normal softening behavior with increasing temperature. C_{44} decreases almost linearly in the whole temperature range, in agreement with experimental observation. The calculated values of shear moduli C_{44} and C' are higher than experimental values [5,6,14], while the bulk modulus comes out lower. The maximum difference between the calculated and experimental moduli is about 30%, which

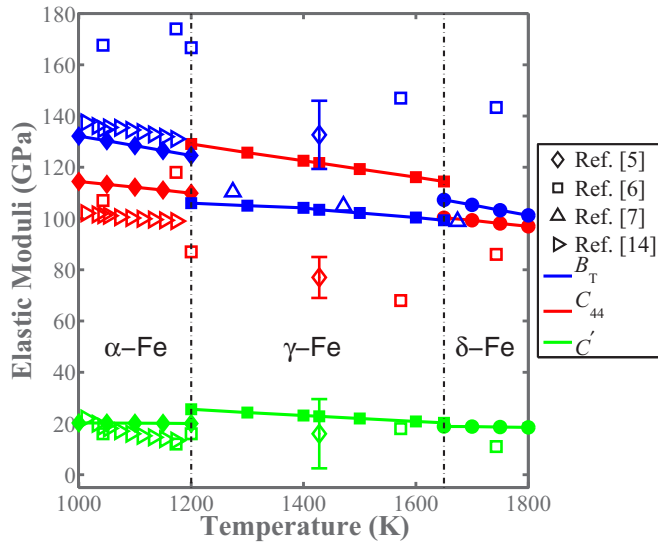


FIG. 6. Calculated temperature dependence of elastic moduli of α -, γ -, and δ -Fe in comparison with experimental data of Refs. [5–7,14]. Blue, red, and green lines represent the variation of B_T , C_{44} , and C' , respectively.

may be called reasonable considering the experimental uncertainties and the fact that the experimental elastic constants of Ref. [5] might not be fully isothermal. Indeed, the experimental bulk modulus of Ref. [5] is considerably higher than the isothermal bulk modulus values obtained in high-pressure measurements of Ref. [7] and in our calculations.

It is also noteworthy that our B_T values are in perfect agreement with the isothermal bulk modulus values measured in Ref. [7] in the whole considered temperature range. As explained in the previous section, a high value of C_{11} obtained in Ref. [6] causes the corresponding bulk modulus to be higher than in other experiments on paramagnetic phases of iron.

IV. CONCLUSIONS

Thermophysical properties of α -, γ -, and δ -Fe at elevated temperatures have been studied using first-principles-based thermodynamic modeling of complex thermal disorder involving electronic, magnetic, and vibrational degrees of freedom. Partial free energy, containing contributions due to the faster degrees of freedom (electronic and magnetic), is evaluated first and then used as the input to model the free-energy contributions from the slower (vibrational) degrees of freedom.

To model the free energy due to vibrational disorder, the quasiharmonic Debye model was employed. To effectively include the contributions from the low- and high-frequency modes in the free energy, we have introduced an averaging technique, the resultant effective direction, that allows one to reliably evaluate the Debye temperature in cases of strong elastic anisotropy.

Good agreement is found between the model predictions for the lattice constant and available experimental data. The calculated lattice constants of α -, γ -, and δ -Fe have been found to be 0.3%, 1.3%, and 0.2% lower than the corresponding experimental values. The difference between the calculated linear TEC and experimental data is 32%, 18%, and 8% for α -, γ -, and δ -Fe, respectively.

According to our calculations, nonphonon contributions to thermal expansion make up about 12% and 10% of the total TEC value for α - and δ -Fe and 30% for γ -Fe. As for heat capacity, our results are in good agreement with experimental data assessed by Desai [48], where there are about 5% and 10% differences for the γ and δ phases, respectively. The present model does not include the effects on magnetic short-range order in paramagnetic α -Fe, and therefore, it does not reproduce the tail of the heat capacity peak above the Curie temperature.

The calculated elastic moduli exhibit a decreasing trend with the increase of temperature. The maximum difference between the calculated elastic moduli and available experimental data is about 30%, which is similar to the results of previous theoretical studies.

The free-energy modeling scheme developed in this work is rather general and computationally very efficient. It can be applied to derive the thermophysical properties of other 3d transition metals and their alloys.

ACKNOWLEDGMENTS

Fruitful discussions with B. Hutchinson and R. Sandström are acknowledged. This work was performed within the VINNEX center Hero-m financed by the Swedish Governmental Agency for Innovation Systems (VINNOVA), Swedish industry, and the KTH Royal Institute of Technology. P.A.K. gratefully acknowledges the financial support of the Ministry of Education and Science of the Russian Federation in the framework of the Increase Competitiveness Program of NUST “MISiS” (Grant No. K3-2017-034). Computer resources for this study were provided by the Swedish National Infrastructure for Computing (SNIC, Project No. 2015/16-50) at the National Supercomputer Center (NSC), Linköping, and PDC Center for High Performance Computing, Stockholm.

- [1] Q. Chen and B. Sundman, *J. Phase Equilib.* **22**, 631 (2001).
- [2] C. Zener, *JOM* **7**, 619 (1955).
- [3] F. Körmann, A. Breidi, S. L. Dudarev, N. Dupin, G. Ghosh, T. Hickel, P. Korzhavyi, J. A. Muñoz, and I. Ohnuma, *Phys. Status Solidi B* **251**, 53 (2014).
- [4] D. Artymowicz, B. Hutchinson, and M. Noguez, *Mater. Sci. Technol.* **18**, 1142 (2013).

- [5] J. Zarestky and C. Stassis, *Phys. Rev. B* **35**, 4500 (1987).
- [6] J. Neuhaus, M. Leitner, K. Nicolaus, W. Petry, B. Hennion, and A. Hiess, *Phys. Rev. B* **89**, 184302 (2014).
- [7] N. Tsujino, Y. Nishihara, Y. Nakajima, E. Takahashi, K. Funakoshi, and Y. Higo, *Earth Planet. Sci. Lett.* **375**, 244 (2013).

- [8] T. Hammerschmidt, I. A. Abrikosov, D. Alfè, S. G. Fries, L. Höglund, M. H. G. Jacobs, J. Koßmann, X.-G. Lu, and G. Paul, *Phys. Status Solidi B* **251**, 81 (2014).
- [9] R. Sandström and P. Korzhavyi, *Can. Metall. Q.* **53**, 282 (2014).
- [10] I. Leonov, A. I. Poteryaev, V. I. Anisimov, and D. Vollhardt, *Phys. Rev. B* **85**, 020401(R) (2012).
- [11] F. Körmann, A. Dick, B. Grabowski, T. Hickel, and J. Neugebauer, *Phys. Rev. B* **85**, 125104 (2012).
- [12] A. V. Ruban and V. I. Razumovskiy, *Phys. Rev. B* **85**, 174407 (2012); A. V. Ruban, V. I. Razumovskiy, and F. Körmann, *ibid.* **89**, 179901(E) (2014).
- [13] I. A. Abrikosov, A. V. Ponomareva, P. Steneteg, S. A. Barannikova, and B. Alling, *Curr. Opin. Solid State Mater. Sci.* **20**, 85 (2016).
- [14] D. J. Dever, *J. Appl. Phys.* **43**, 3293 (1972).
- [15] H. Zhang, B. Johansson, and L. Vitos, *Phys. Rev. B* **84**, 140411(R) (2011).
- [16] Z. Dong, W. Li, S. Schönecker, S. Lu, D. Chen, and L. Vitos, *Phys. Rev. B* **92**, 224420 (2015).
- [17] K. Wildberger, P. Lang, R. Zeller, and P. H. Dederichs, *Phys. Rev. B* **52**, 11502 (1995).
- [18] N. D. Mermin, *Phys. Rev.* **137**, A1441 (1965).
- [19] R. J. Weiss and K. J. Tauer, *Phys. Rev.* **102**, 1490 (1956).
- [20] G. Grimvall, *Phys. Rev. B* **39**, 12300 (1989).
- [21] S. Shallcross, A. E. Kissavos, V. Meded, and A. V. Ruban, *Phys. Rev. B* **72**, 104437 (2005).
- [22] S. V. Okatov, Y. N. Gornostyrev, A. I. Lichtenstein, and M. I. Katsnelson, *Phys. Rev. B* **84**, 214422 (2011).
- [23] P. Soven, *Phys. Rev.* **156**, 809 (1967).
- [24] B. L. Gyorffy, *Phys. Rev. B* **5**, 2382 (1972).
- [25] B. L. Gyorffy, A. J. Pindor, J. B. Staunton, G. M. Stocks, and H. Winter, *J. Phys. F* **15**, 1337 (1985).
- [26] H. Ebert, S. Mankovsky, K. Chadova, S. Polesya, J. Minár, and D. Ködderitzsch, *Phys. Rev. B* **91**, 165132 (2015).
- [27] L. Vitos, P. A. Korzhavyi, and B. Johansson, *Phys. Rev. Lett.* **96**, 117210 (2006).
- [28] V. I. Razumovskiy, A. V. Ruban, and P. A. Korzhavyi, *Phys. Rev. Lett.* **107**, 205504 (2011).
- [29] N. M. Rosengaard and B. Johansson, *Phys. Rev. B* **55**, 14975 (1997).
- [30] A. V. Ruban, S. Khmelevskiy, P. Mohn, and B. Johansson, *Phys. Rev. B* **75**, 054402 (2007).
- [31] A. V. Ruban, A. B. Belonoshko, and N. V. Skorodumova, *Phys. Rev. B* **87**, 014405 (2013).
- [32] A. V. Ruban and M. Dehghani, *Phys. Rev. B* **94**, 104111 (2016).
- [33] Z. Dong, W. Li, D. Chen, S. Schönecker, M. Long, and L. Vitos, *Phys. Rev. B* **95**, 054426 (2017).
- [34] F. Pan, J. Chico, A. Delin, A. Bergman, and L. Bergqvist, *Phys. Rev. B* **95**, 184432 (2017).
- [35] P.-W. Ma, S. L. Dudarev, and J. S. Wróbel, *Phys. Rev. B* **96**, 094418 (2017).
- [36] O. Hellman, P. Steneteg, I. A. Abrikosov, and S. I. Simak, *Phys. Rev. B* **87**, 104111 (2013).
- [37] P. Hohenberg and W. Kohn, *Phys. Rev. B* **136**, B864 (1967).
- [38] J. P. Perdew, K. Burke, and M. Ernzerhof, *Phys. Rev. Lett.* **77**, 3865 (1996).
- [39] L. Vitos, H. L. Skriver, B. Johansson, and J. Kollar, *Comput. Mater. Sci.* **18**, 24 (2000).
- [40] L. Vitos, *Phys. Rev. B* **64**, 014107 (2001).
- [41] L. Vitos, I. A. Abrikosov, and B. Johansson, *Phys. Rev. Lett.* **87**, 156401 (2001).
- [42] L. Vitos, *Computational Quantum Mechanics for Materials Engineers* (Springer, London, 2007).
- [43] H. J. Monkhorst and J. D. Pack, *Phys. Rev. B* **13**, 5188 (1976).
- [44] O. L. Anderson, in *Physical Acoustics*, edited by W. P. Manson (Academic Press, New York, 1965), Vol. **IIIB**, pp. 43–95.
- [45] V. L. Moruzzi, J. F. Janak, and K. Schwarz, *Phys. Rev. B* **37**, 790 (1988).
- [46] Z. S. Basinski, W. Hume-Rothery, and A. L. Sutton, *Proc. R. Soc. London, Ser. A* **229**, 459 (1955).
- [47] P. Haas, F. Tran, and P. Blaha, *Phys. Rev. B* **79**, 085104 (2009).
- [48] P. D. Desai, *J. Phys. Chem. Ref. Data* **15**, 967 (1986).
- [49] M. J. Mehl, B. M. Klein, and D. A. Papaconstantopoulos, in *Intermetallic Compounds: Principles and Practice*, edited by J. H. Westbrook and R. L. Fleischer (Wiley, London, 1994), pp. 195–210.